DOT/FAA/AR-xx/xx

Office of Aviation Research
and Development
Washington, DC 20591

FAA Development Of Reliable Modeling Methodologies For Fan Blade Out Containment Analysis Part 2: Ballistic Impact Testing

Date

Type of Report

This document is available to the public through the National Technical Information Service (NTIS), Springfield, Virginia 22161.

U.S. Department of Transportation
Federal Aviation Administration

NOTICE

This report is available at the Federal Aviation Administration William J. Hughes Technical Center's Full-Text Technical Reports page: actlibrary.tc.faa.gov in Adobe Acrobat portable document format (PDF).

Technical Report Documentation Page

1. Report No.	2. Government Accession No.	3. Recipient's Catalog No.
DOT/FAA/(AR)-xx/xx		

4. Title and Subtitle	5. Report Date
FAA DEVELOPMENT OF RELIABLE MODELING METHODOLOGIES FOR FAN BLADE OUT CONTAINMENT ANALYSIS Part 2: BALLISTIC IMPACT TESTING	
	6. Performing Organization Code
7. Author(s) Duane M. Revilock and J. Michael Pereira	8. Performing Organization Report No.
9. Performing Organization Name and Address NASA Glenn Research Center 21000 Brookpark Road Cleveland, OH 44135	10. Work Unit No. (TRAIS)
	11. Contract or Grant No.
12. Sponsoring Agency Name and Address U.S. Department of Transportation Federal Aviation Administration Office of Aviation Research and Development Washington, DC 20591	13. Type of Report and Period Covered
	14. Sponsoring Agency Code

15. Supplementary Notes

.

16. Abstract

This report summarizes the ballistic impact testing that was conducted to provide validation data for the development of numerical models of blade out events in fabric containment systems. The ballistic impact response of two different fiber materials - Kevlar 49 (E.I. DuPont Nemours and Company) and Zylon AS (Toyobo Co., Ltd.) was studied by firing metal projectiles into dry woven fabric specimens using a gas gun. The shape, mass, orientation and velocity of the projectile were varied and recorded. In most cases the tests were designed such that the projectile would perforate the specimen, allowing measurement of the energy absorbed by the fabric. The results for both Zylon and Kevlar presented here represent a useful set of data for the purposes of establishing and validating numerical models for predicting the response of fabrics under conditions simulating those of a jet engine blade release situations. In addition some useful empirical observations were made regarding the effects of projectile orientation and the relative performance of the different materials.

17. Key Words	18. Distribution Statement
	This document is available to the U.S. public through the National Technical Information Service (NTIS), Springfield, Virginia 22161.

19. Security Classif. (of this report)	20. Security Classif. (of this page)	21. No. of Pages	22. Price
Unclassified	Unclassified		

LIST OF FIGURES

LIST OF TABLES

Note: If a title in the table of contents, list of figures, or list of tables carries over to a second line, leave a blank line between all entries. Otherwise, single-space all entries (as shown above).

LIST OF ACRONYMS

FAA	Federal Aviation Administration
NASA	National Aeronautics and Space Administration

Note: Acronyms should be defined at the first occurrence in the text only if the acronym is subsequently used within the report. If it is not used more than once, then the acronym should be spelled out (for example, if the acronym FAA is used only once, then use Federal Aviation Administration).

All acronyms are required to be defined in the abstract, executive summary, body of the report, conclusions, and in each appendix.

TABLE OF CONTENTS

EXECUTIVE SUMMARY

A team consisting of Arizona State University, Honeywell Engines & Systems, NASA Glenn Research Center and SRI International collaborated to develop computational models and verification testing for designing and evaluating turbine engine fan blade fabric containment structures. This research was conducted under the Federal Aviation Administration's Airworthiness Assurance Center of Excellence and sponsored by the Aircraft Catastrophic Failure Prevention Program. The research was directed towards improving the modeling of a turbine engine fabric containment structure for an engine blade-out containment demonstration test required for certification of aircraft engines.
In the first phase of this research work [1,2,3,4], much progress was made in testing and computational analysis. A fabric material model was developed for Kevlar and Zylon fabrics. Static testing of containment wraps subjected to loads through a blunt nose impactor was carried out at ASU. Ballistic testing of containment wraps subjected to a high velocity blunt projectile was carried out at NASA-Glenn. These tests have provided test cases (benchmark results) to validate the developed finite element methodology. While the work performed in the previous research program met the stated objectives, improvements in robustness and confidence of the finite element simulations and predictions was desired.

The research conducted in this second phase brings a new level of capability to design and develop fan blade containment systems for turbine engines. To achieve the program objectives, a plan consisting of four technical tasks was developed and implemented as follows:

Task 1: Robust FE Model Development-The objective of this task was to increase confidence and robustness in the material models for the Kevlar and Zylon material models developed in phase 1.

Task 2: Improve FE Modeling Capability for Multiple Layers of Fabric-In Phase I program, most of the LS-DYNA models used a single element through the thickness to model the fabric, which ranged from one to twenty four layers.

Task 3: 1500 denier (d) Zylon® Material Model Development-In the previous program, limited ballistic and static tests of 1500d Zylon indicated this configuration of Zylon might have the potential to offer a 60 percent weight advantage over a similar configuration of Kevlar 49 fabric for the same fragment energy. The objective of this task was to develop and validate a material model for 1500 Denier Zylon. It should be noted that during the conduct of this study, it was discovered that Zylon was found have excessive deterioration due to heat and humidity. As a result of this, it was decided that the remainder of this study would focus only on Kevlar fabrics.

Task 4: Engine Simulations-As in the previous program, the objective of this task was to validate improvements to the material models and FE methods developed under this program as they relate to propulsion engine fan blade containment. Existing fabric material models and modeling methods and improvements to the material models and methods were validated using fan containment test data.

Each member of the team took a leadership role and developed a comprehensive report describing the details of the research task and the findings. The comprehensive report is made up of four report parts. These reports are as follows:

1) Arizona State University Department of Civil Engineering, Part 1: Fabric Material Tests
2) NASA-Glenn Research Center, Part 2: Ballistic Testing
3) SRI International, Part 3: Material Model Development and Simulation of Experiments
4) Honeywell Engines, Systems and Services, Part 4: Model Simulation for Ballistic Tests, Engine Fan Blade-Out and Generic Engine Model

This report contains a description of and results from Part 2 of this project, the ballistic impact testing conducted at NASA Glenn Research Center.

1. INTRODUCTION

In the last thirty years the use of aramid fabrics in jet engine blade containment systems has become common. It is recognized that high strength and high elongation fabrics, combined with innovative structural concepts can provide a light weight, effective fan case system that provides the strength required to safely handle impact loads, blade rub loads and the large dynamic loads caused by rotor imbalance. Aramid and other high strength fibers and fabrics have been studied extensively due to their application in a wide range of products such as bullet-proof vests, cut-resistant gloves, tires and sports equipment. However, relatively small amounts of data exist in the public domain for the impact response of fabrics in configurations that are similar to those used in jet engine applications.

Containment design is currently largely based on empirical methods but there is strong motivation on the part of jet engine manufacturers to develop numerical models that can be used to help in the design process of fan containment systems, thereby reducing the cost of testing and increasing confidence and reliability in the design. A number of research and commercial computer programs are available that can simulate the impact of a released fan blade on the case (a blade-out event). These are generally transient, explicit integration finite element codes [5, 6]. The codes themselves are accurate and have been validated by years of use but the constitutive, failure and contact models are still the subjects of active research. A large body of data and research studies exist with regard to high strain rate behavior and impact response and constitutive and failure models for metals [7, 8, 9]. While there is data available in the literature on the impact response of fabrics [10, 11, 12], and models have been developed to simulate fabric impact response [13, 14, 15] the body of literature is much smaller than for metals. In addition, studies tend to focus on applications other than jet engines (such as body armor) and generally consider impacts by small high velocity projectiles. Jet engine fan containment impact involves a larger projectile at sub-sonic velocities.

To address the lack of data and to improve the material models in the range of jet engine applications, the Federal Aviation Administration (FAA) recently completed a project aimed at developing improved computational tools for designing fabric-based engine containment systems [1, 2, 3, and 4]. This study was done on Kevlar 49® and Zylon® as spun (AS) fabric and involved static testing and modeling, conducted by The Arizona State University, ballistic impact testing of fabric rings, conducted by the NASA Glenn Research Center, material model development and simulation of experiments, conducted by SRI International and model simulations of ballistic tests, fan blade-out and generic engine modeling conducted by Honeywell Engines Systems and Services.

As a follow-up to that work, a second phase was conducted with the objective of increasing the confidence and robustness of the material models. This involved additional finite element model development and additional static and ballistic impact testing. This report summarizes the ballistic impact testing that was conducted to provide validation data for the numerical model development. In addition some useful empirical

observations were made regarding the effects of projectile orientation and the relative performance of the different materials.

2. METHODS

The ballistic impact response of fabrics was studied by firing metal projectiles into dry woven fabric specimens using a gas gun. The shape, mass, orientation and velocity of the projectile were varied and recorded. In most cases the tests were designed such that the projectile would perforate the specimen, allowing measurement of the energy absorbed by the fabric.

2.1 MATERIALS

Fabrics woven from two different fiber materials - Kevlar 49 (E.I. DuPont Nemours and Company) and Zylon AS (Toyobo Co., Ltd.) - were tested. Kevlar is an aramid material with a long history in impact applications in general and fan containment systems in particular [16, 17]. Zylon has been under development more recently. A number of studies have demonstrated that, when stored and tested under laboratory conditions, Zylon demonstrates superior performance over Kevlar [18, 19]. This study considered a single fabric architecture for Kevlar and two architectures for Zylon. The fibers and architecture were selected so that two materials of similar architecture were compared, and two different architectures of the same material (Zylon) were compared. The fiber and weave parameters of the materials tested are shown in Table 1 [14].

2.2 TEST CONFIGURATION

The test specimens consisted of layers of 0/90 plain woven cloth, 25 cm (10 in) wide, wrapped around a ring shaped fixture as shown in Figure 1. The fixture was steel and had an outer diameter of 102 cm (40 in), a thickness of 2.5 cm (1 in) and a height the same as the fabric width (25 cm). The fabric was rolled around the fixture under a controlled tension of 25 N (5.5 lb) to make up the desired number of layers. The fixture had a 25.4 cm (10 in) circumferential gap at the impact location. It was placed in front of the gun barrel at an incline of 15º so that the projectile, after exiting the gun barrel, passed over the front edge of the ring, passed through the gap in the ring fixture and impacted the fabric from the general direction of the center of the ring. Because of the circumferential gap, and the tension on the specimen, the fabric was flat at the region where impact occurred, rather than following the curved shape of the ring fixture. This configuration was chosen rather than a flat specimen held in a square or

Figure 1. Fabric Specimen Wrapped Around Ring Fixture. Arrow Shows the Location of Impact.

Table 1. Fabric Properties

		Zylon AS Poly-benzobisoxazol (PBO)		Kevlar-49 P-Aramid
		Light	Heavy	Standard
Volume Density	(g/cm^3)	1.54	1.54	1.44
Yarn Denier (measured) [3]	(g/9km)	500	1500	1490
Yarn Linear Density	(mg/cm)	0.556	1.654	1.656
Yarn count	(yarns/in)	35x35	17x17	17x17
Yarn count	(yarns/cm)	13.8x13.8	6.7x6.7	6.7x6.7
Fabric ply thickness	(mm)	0.21	0.28	0.28
Fabric areal density	(g/cm^2)	.01575	.0223	.02275
Degree of Crimp Warp Yarns	(%)	3.1	2.2	1.1
Degree of Crimp Fill Yarns	(%)	0.6	0.9	0.8

rectangular fixture because experience has shown that that in this latter configuration the boundary conditions play a major role in the response of the fabric specimen.

Three different projectiles were used in this study. The first was a rectangular shaped, 304L stainless steel article, 10.2 cm (4 in) long, 5.1 cm (2 in) high and 0.8 cm (5/16 in) thick (Figure 2), with a nominal mass of 320 gm. The front edge and the corners of the projectile were machined with a full radius. This projectile was designated Projectile A. This is the same projectile as was used in Phase I of this program [2]. The second projectile was also 304L stainless steel, but had a length of 17.8 cm (7 in), a height of 3.8 cm (1.5 in), a thickness of 0.60 cm (.235 in) and the same nominal mass as Projectile A. The front edge and corners also were machined with a full radius (Figure 2). The second projectile was designated Projectile B. The third projectile which was used in only two tests was the same as projectile A, but measured 6 inches in length instead of 4 inches. The third projectile was designated Projectile C.

The gas gun used to accelerate the projectile consisted of a pressure vessel with a volume of 0.35 m^3 (12.5 ft^3), a gun barrel with a length of 12.2 m (40 ft) and an inner diameter of 20.32 cm (8 in). A photograph of the gun is shown in Figure 3. The pressure vessel and the gun barrel were mated by a flange on each side with a number of layers of Mylar® sheet sandwiched between the flanges to seal the pressure vessel and act as a burst valve. Helium gas was used as the propellant. The pressurized helium was released into the gun barrel by applying a voltage across a Nichrome wire embedded in the Mylar sheets, causing the Mylar sheets to rupture. The projectile was supported inside an aluminum can-shaped cylindrical sabot that was machined to fit snugly inside the gun barrel. The orientation of the projectile was controlled by supporting the projectile either with rigid foam or with an aluminum wedge welded to the bottom of the sabot. The sabot was stopped at the end of the gun barrel by a thick steel plate with a rectangular slot large enough to allow the projectile to pass through. The gun barrel was evacuated to reduce blast loading on the specimen and to reduce the amount of pressure required to achieve the desired impact velocity.

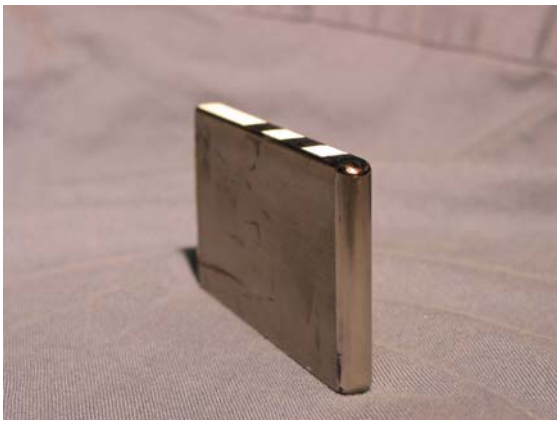

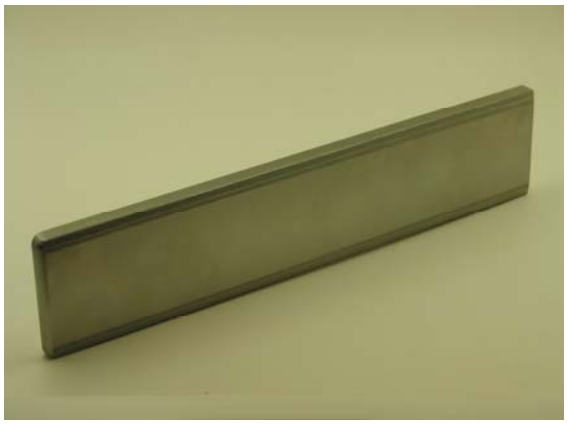

Figure 2. Stainless Steel Projectiles (Left View - Projectile A; Right View - Projectile B)

Figure 3. Gas Gun Used for Ballistic Impact Testing

A number of different high-speed digital video cameras were used to obtain both qualitative and quantitative information from each test. Figure 4 shows sequences of still images obtained from two Phantom 7 cameras (Vision Research, Inc.). The impact velocity and exit velocity were measured using the digital video cameras. The orientation of the projectile was measured from the location of three points on the projectile that defined a local moving coordinate system and three points at a fixed location in the background that defined a laboratory coordinate system. The laboratory coordinate system consisted of the X axis in the direction of the gun axis, a Z axis in the vertical upward direction and a Y axis defined by the vector product of Z and X. The orientation of the projectile was defined by a set of three Euler angles defined by a rotation θ (roll), about the laboratory X axis, followed by a rotation ψ (pitch) about the rotated y-axis, followed by a rotation φ (yaw) about the (twice) rotated z-axis. The coordinate systems are shown in Figure 5. The positions of the points that defined the coordinate systems were measured using a stereo imaging system (PONTOS, GOM mbH) coupled with a pair of calibrated Phantom 5 high-speed digital video cameras (Vision Research, Inc). The Euler angles were computed by defining the unit vectors in each of the two coordinate systems, forming the direction cosine matrix and equating the direction cosine matrix to the coordinate transformation matrix (Appendix A).

2.3 TEST MATRIX

Three sets of tests were conducted in this program. The first set consisted of tests in which the orientation and aspect ratio of the projectile were varied from those conducted in the Phase I program [2]. In the second set of tests additional data were taken on 1500 denier Zylon in the same test configuration as the Phase I program. A final set of two tests was conducted on a fabric ring in which there was essentially no tension on the fabric.

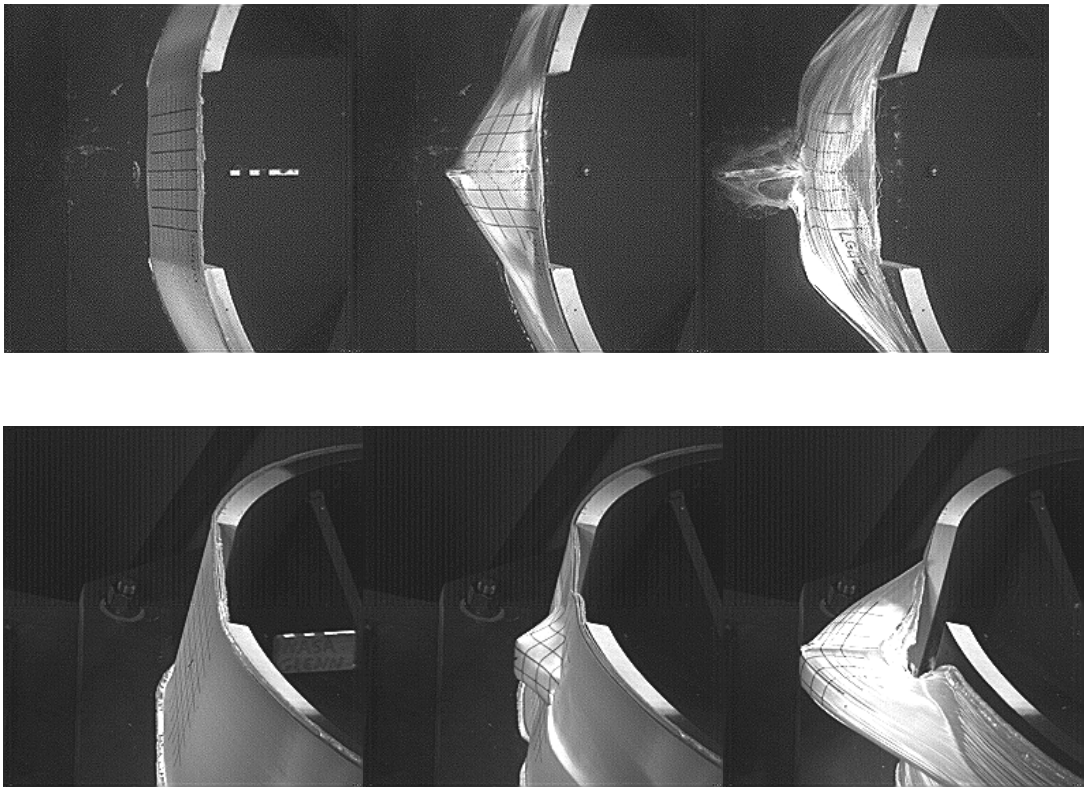

Figure 4. Three Still images from typical tests. Top and Side Views.

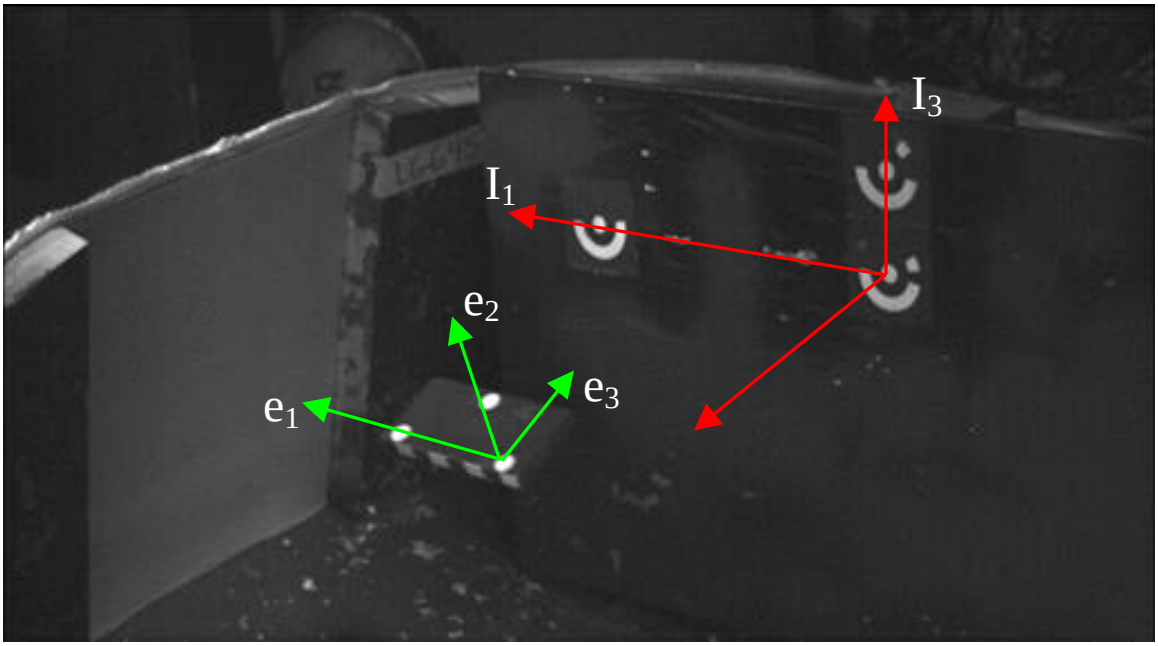

Figure 5. Projectile During Flight. The Local and Laboratory Coordinate Systems are Shown.

3. RESULTS

A total of 46 successful impact tests were conducted. A test was considered successful if the velocity before and after impact and the orientation at the impact point could be accurately measured. Results for the first set of tests, in which the projectile orientation and aspect ratio were varied, are shown in Table 2. It was not possible to control the orientation of the projectile such that it exactly matched the desired orientation, and in some cases there was considerable deviation.

The amount of energy absorbed by the fabric was highly dependent on the orientation of the projectile at impact. While no correlation was found between the roll angle and the energy absorbed, there was a dependency on both pitch and yaw angles. Figure 6 shows the energy absorbed, normalized by the overall fabric specimen areal weight, as a function of the absolute value of the projectile yaw angle for the tests shown in Table 2. It can be observed that the absorbed energy to increases as the absolute value of the yaw angle increases. The figure shows that the Zylon material absorbs more energy overall, and that as the yaw angle increases the effectiveness of the 500 denier Zylon approaches that of the 1500 denier Zylon. It may be hypothesized that as the yaw angle increases and the projectile appears less sharp, the energy absorption is less localized and the architecture of the fabric plays a less important role.

The yaw angle of the projectile has the biggest effect of the three angles on the projected area of the projectile on the fabric. The projected area of the projectile can be computed

Test No.	File No.	Fabric		Penetrator	Fabric Layers	Penetrator Mass (gm)	Desired Configuration Pitch (deg)	Roll (deg)	Yaw (deg)	Actual Configuration Pitch (deg)	Roll (deg)	Yaw (deg)	Before Impact Velocity (ft/sec)	Energy Joules	After Impact Velocity (ft/sec)	Energy (Joules)	Absorbed Energy (Joules)	%	Presented Area (cm^2)	Specimen Areal Mass (gm/cm^2)
1	LG572	Kevlar	11/10/2004	A	8	319.68	0	0	0	21	0	13	346.6	1783.908	294.95	1291.85	492.0579	0.275831	1.455883	0.182
2a	LG688	Kevlar	8/18/2005	A	8	317.78	0	0	45	-20.52	10.47	62.78	870.93	11196.78	549.33	4454.44	6742.336	0.602168	7.368006	0.182
2b	LG689	Kevlar	8/18/2005	A	8	323.24	0	0	45	-1.28	-12.83	49.72	896.26	12061.27	655.08	6443.379	5617.891	0.465779	6.695206	0.182
4a	LG611	Kevlar	3/17/2005	A	8	321.2	0	45	0	-1.74	30.89	-10.78	905.68	12238.41	798.05	9502.452	2735.959	0.223555	2.968875	0.182
4b	LG612	Kevlar	3/18/2005	A	8	321.01	0	45	0	-3.74	22.78	-0.53	898.25	12031.31	822.73	10093.3	1938.011	0.161081	8.671523	0.182
5c	LG692	Kevlar	8/22/2005	A	8	315.95	0	45	45	2.31	38.24	41.45	885.32	11503.2	602.56	5328.671	6174.534	0.536766	29.5295	0.182
11b	LG594	Kevlar	2/14/2005	B	8	306.77	0	0	45	6.6	27	47.8	843.85	10147.13	484.5	3345.033	6802.1	0.670347	43.74875	0.182
13a	LG609	Kevlar	3/16/2005	B	8	304.87	0	45	0	0.87	37.35	1.63	913.72	11823.36	825.42	9648.607	2174.753	0.183937	11.05101	0.182
13b	LG610	Kevlar	3/17/2005	B	8	306.82	0	45	0	0.7	25.3	11.93	888.09	11240.81	809.69	9343.749	1897.06	0.168765	8.428553	0.182
14a	LG618	Kevlar	4/6/2005	B	8	305.5	0	45	45	6.31	-47.14	51.55	866.42	10652.91	558.91	4432.971	6219.935	0.583872	60.17142	0.182
14b	LG620	Kevlar	4/11/2005	B	8	316.2	0	45	45	0.18	-37.79	55.07	893.83	11734.69	580.78	4954.332	6780.359	0.577805	62.03371	0.182
37a	LG655	Kevlar	7/8/2005	A	32	313.05	0	0	0	1.29	-32.46	2.57	1131.72	18624.8	830.6	10032.23	8592.57	0.461351	12.41755	0.728
37b	LG656	Kevlar	7/8/2005	A	32	321.57	0	0	0	-2.31	8.98	-10.07	967.31	13976.77	469.24	3289.012	10687.76	0.76468	13.88781	0.728
37c	LG657	Kevlar	7/18/2005	A	32	325.35	0	0	0	9.73	-22.16	1.42	829.71	10404.07	0	0	7673.78	1	9.234865	0.728
22a	LG613	1500 Zylon	3/24/2005	A	8	325.87	0	45	0	-1.6	30.91	-2.62	876.42	11627.03	495.9	3722.481	7904.551	0.679843	12.17925	0.1784
29a	LG599	1500 Zylon	2/22/2004	B	8	310.63	0	0	45	13.54	10.24	38.34	873.81	11017.36	22.66	7.40906	11009.95	0.999328	36.78507	0.1784
29b	LG600	1500 Zylon	2/23/2004	B	8	311.84	0	0	45	-0.59	-23.16	51.93	866.11	10866.2	158.61	364.4122	10501.79	0.966464	58.16556	0.1784
31b	LG608	1500 Zylon	3/15/2005	B	8	306.16	0	45	0	-0.21	46.12	-1.83	859.58	10508.02	562.83	4505.084	6002.939	0.571272	16.9953	0.1784
32b	LG617	1500 Zylon	4/4/2005	B	8	306.54	0	45	45	-4.94	-44.06	-54.78	871.94	10825.81	249.24	884.5504	9941.257	0.918292	49.38487	0.1784
20b	LG690	500 Zylon	8/19/2005	A	8	323.59	0	0	45	-13.34	-24.45	39.27	895.65	12057.9	654.22	6433.431	5624.469	0.466455	39.79237	0.126
22a	LG626	500 Zylon	5/6/2005	A	8	315.06	0	45	0	-5.2	25.1	-6.3	901.35	11889.95	786.12	9044.215	2845.737	0.23934	14.23258	0.126
22b	LG627	500 Zylon	5/6/2006	A	8	322.72	0	45	0	-8.5	33.2	-10.4	816.02	9982.226	650.16	6336.746	3645.48	0.365197	19.42487	0.126
22b	LG639	500 Zylon	6/7/2005	A	8	326.58	0	45	0	-7.35	61.33	9.17	934.58	13250.2	809.81	9948.458	3301.743	0.249184	6.592087	0.126
23a	LG694	500 Zylon	8/23/2005	A	8	322.96	0	45	45	1.97	80.57	52.87	900.28	12159.17	560.35	4710.504	7448.664	0.612596	34.74092	0.126
23b	LG695	500 Zylon	8/23/2005	A	8	316.39	0	45	45	-0.73	37	50.02	905.9	12061	569.9	4773.314	7287.683	0.604236	36.16893	0.126
25a	LG644	500 Zylon	6/21/2005	A	8	325.1	0	90	0	-3.79	88.19	-1.86	910.67	12523.88	842.93	10730	1793.877	0.143236	17.99141	0.126
25b	LG645	500 Zylon	6/22/2005	A	8	316.09	0	90	0	-1.86	68.77	0.45	917.25	12353.39	824.82	9989.162	2364.227	0.191383	15.09019	0.126
28a	LG640	500 Zylon	6/8/2005	B	8	306.38	0	0	0	0.077	-6.4	-2.66	885.3067	11154.44	829.77	9798.866	1355.575	0.121528	3.357609	0.126
28b	LG641	500 Zylon	6/9/2005	B	8	306.17	0	0	0	6.98	2.74	7.83	892.28	11323.09	835.66	9931.659	1391.429	0.122884	10.002	0.126
31a	LG642	500 Zylon	6/9/2005	B	8	310.3	0	45	0	1.42	44.32	1.03	904.89	11802.48	849.19	10394.21	1408.271	0.11932	13.35066	0.126
31b	LG643	500 Zylon	6/10/2005	B	8	306.4	0	45	0	-4.68	44.85	-1.16	894.16	11379.39	779.23	8642.115	2737.28	0.240547	15.9766	0.126
39a	LG658	500 Zylon	7/19/2005	A	32	321.77	0	0	0	4.95	-8.96	0.38	1130.42	19099.64	939.77	13200.45	5899.192	0.308864	5.434402	0.504
39b	LG659	500 Zylon	7/19/2005	A	32	321.5	0	0	0	2.12	6.81	5.28	1023.47	15643.4	706.15	7446.888	8196.511	0.52396	5.994404	0.504
39c	LG660	500 Zylon	7/20/2005	A	32	326.78	0	0	0	-8.99	-5.01	-0.16	967.67	14213.79	549.15	4577.595	9636.197	0.677947	4.055432	0.504

Table 2 Results from Impact Tests with Varying Projectile Orientation and Aspect Ratio

from the planar area of the projectile multiplied by the scalar product of the unit vectors normal to the projectile and normal to the fabric. That is,

$$A_p = A(\vec{e}_2 \cdot \vec{i}_n) \tag{1}$$

Where A_p is the projected area of the projectile, A is the planar area of the projectile, $\vec{e}_2$ is the unit normal vector to the projectile (Figure 5) and $\vec{i}_n$ is the unit normal to the fabric specimen at the impact point. In this case, $\vec{i}_n = \vec{I}_1 \cos(15) + \vec{I}_3 \sin(15)$ where $\vec{I}_1$ and $\vec{I}_3$ are shown in Figure 5.

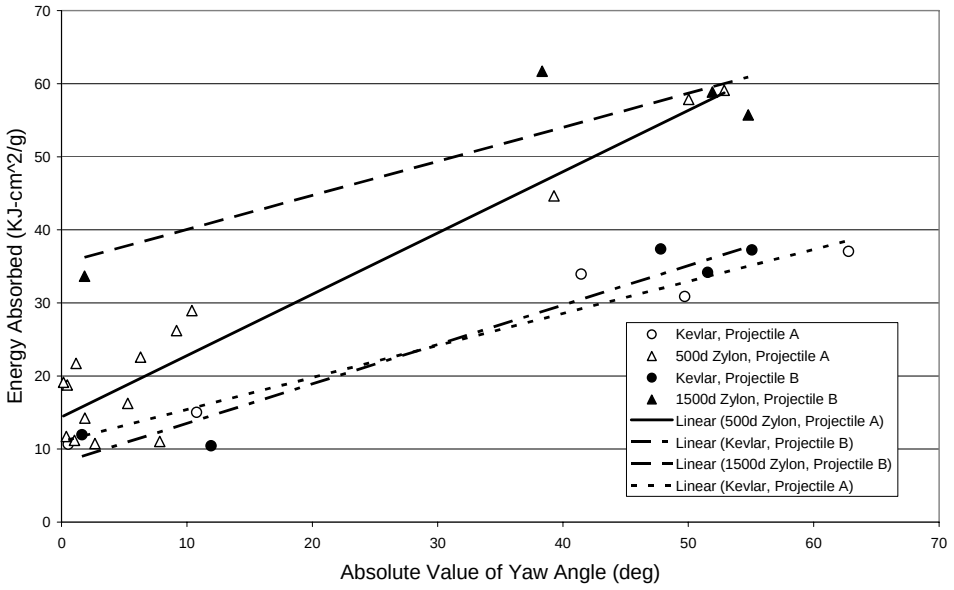

Figure 6. Normalized Absorbed Energy as a Function of the Projectile Yaw Angle

The effect of the projectile projected area on the energy absorbed, normalized by the total areal weight of the fabric specimen, is shown in Figure 7 for the Kevlar and 1500 denier Zylon. While there is some scatter in the results, there appears to be a linear relationship between the normalized energy absorbed and the projected area of the projectile. In addition, it appears that the actual shape of the projectile had less of an effect than the presented area itself. It can also be seen in Figure 7 that the normalized energy absorbed by Zylon is approximately twice as that by Kevlar of the same areal weight and architecture.

One of the objectives of this study was to expand upon the Phase I results for 1500 denier Zylon [2] to verify the enhanced performance over Kevlar. This involved a number of

impact tests in which the nominal orientation of the projectile was (0, 0, 0) pitch, roll and yaw (Table 3). Figure 8 shows the normalized energy for the 1500 denier Zylon from the two sets of experiments, as well as the earlier phase I results for Kevlar. The material from the present study (Phase II) did not perform as well as that from the earlier study (Phase I). However, both sets of Zylon absorbed significantly more energy than Kevlar.

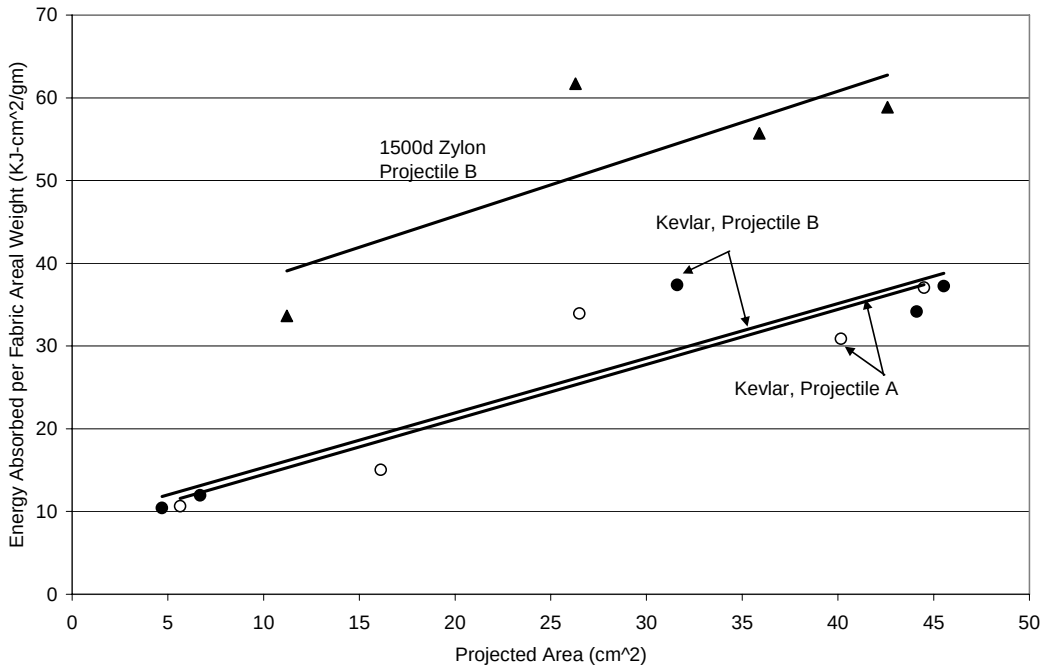

Figure 7 Normalized Absorbed Energy as a Function of the Projectile Projected Area

The difference in impact strength between Phase I and Phase II for the 1500 denier Zylon was considered significant and worthy of investigation. It was hypothesized that the difference was due to the known age related degradation in the mechanical properties of the Zylon. In Phase I of this study [2] the 1500 denier Zylon was fabricated in March, 2002 and the impact testing was conducted between May 9 and May 21, 2002, a period of two to three months. In the Phase II study the material was manufactured in June, 2004 and the impact testing was conducted between July 21 and Aug. 30, 2005, over a year later. During the period between manufacture and testing in both phases the material was stored under normal indoor laboratory conditions in a closed container to prevent any light.

A test program was conducted at the ASU Department of Civil Engineering to investigate age-related changes in strength, modulus and toughness of 1500 denier Zylon stored under laboratory conditions. A summary of this study is included in Appendix B of this report. The study concluded that there is a statistically significant decrease in the strength and toughness of the fabric with age, and a small decrease in the stiffness. Over a 12 month period the strength decreased by 9% and the toughness decreased by 22%. The stiffness decreased by 2%. In addition, tests conducted on virgin fabric 8 months

after delivery to the fabric weaver showed a 40% decrease in the measured strength compared to the manufacturer's published value. These results support the hypothesis that the reduction in the impact energy absorption capacity of the 1500 denier Zylon between Phase I and Phase II was, in fact, due to age-related changes in mechanical properties.

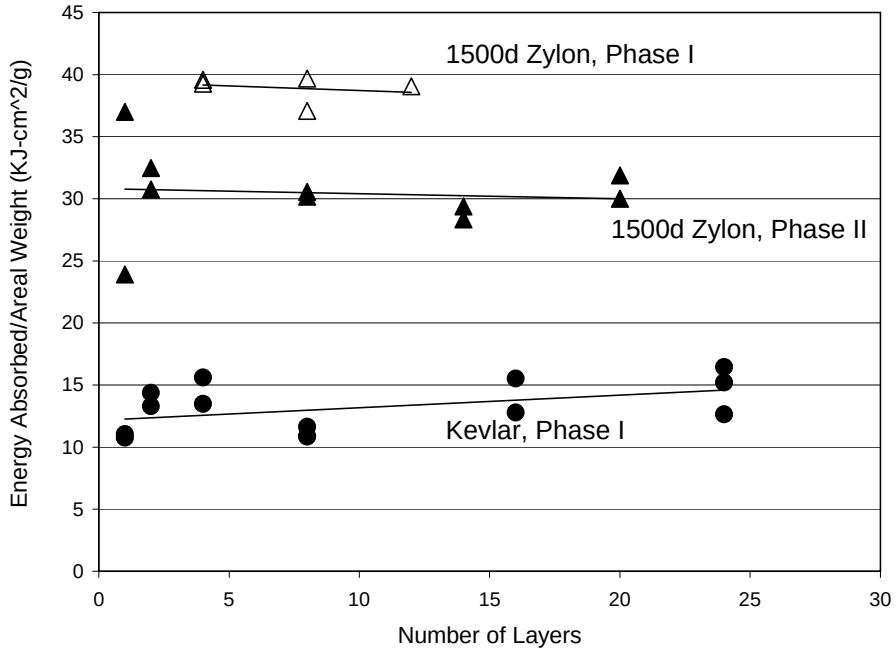

Figure 8. Normalized Energy Absorbed as a Function of the Number of Fabric Layers. Results of This Study (Phase II) Compared With Those in Phase I

The final set of tests was performed to look at the effect of fabric tension. In these tests eight layers of 500d Zylon were wrapped around the fixture with essentially no tension and impacted using projectile A with a desired orientation of (0, 0, 0) pitch, roll and yaw respectively. The results of these tests are shown in Table 4. The results were compared with the 500d Zylon tests (Projectile A) from Table 2 and are shown in Figure 9. Figure 9 shows the increase in absorbed energy per unit fabric total areal weight as a function of projectile projected area for the specimens under the nominal tension. Results from the two tests at low tension show no significant difference. However, it should be noted that only two tests were conducted at low specimen tension and more tests are needed to gain more confidence in this conclusion.

Test No.	Fabric	Penetrator	Test Date	Fabric Layers	Penetrator Mass (gm)	Actual Configuration Pitch (deg)	Roll (deg)	Yaw (deg)	Before Impact Velocity (ft/sec)	Energy (ft-lb)	After Impact Velocity (ft/sec)	Energy (ft-lb)	Absorbed Energy (ft-lb)	%
LG661	1500 Zylon	A	7/21/2005	8	320.57	-13.59	1.25	3.25	886.97	8640.657	652.07	4670.005	3970.652	0.459531
LG663	1500 Zylon	A	7/22/2005	8	321.59	2.64	-27.19	3.56	875.97	8454.483	634.38	4434.121	4020.362	0.47553
LG662	1500 Zylon	A	7/21/2005	1	325.6	-6.41	-48.01	-4.98	623.74	4340.079	578.36	3731.53	608.549	0.140216
LG664	1500 Zylon	A	7/22/2005	1	326.76	1.69	-3.37	0.52	615.03	4234.748	585.78	3841.528	393.2195	0.092855
LG698	1500 Zylon	A	8/25/2005	2	323.77	0.47	-13.19	4.94	597.4192	3959.141	515.4869	2947.664	1011.478	0.255479
LG702	1500 Zylon	A	8/31/2005	2	320.23	0.51	11.55	10.59	604.0339	4003.046	517.2067	2934.92	1068.126	0.266828
LG700	1500 Zylon	A	8/26/2005	14	318.46	2.32	12.06	-2.75	1012.456	11184.42	653.473	4659.253	6525.165	0.583416

Table 3. Results of Impact Tests on 1500d Zylon

Test No.	Fabric	Penetrator	Test Date	Fabric Layers	Penetrator Mass (gm)	Actual Configuration Pitch (deg)	Roll (deg)	Yaw (deg)	Before Impact Velocity (ft/sec)	Energy (Joules)	After Impact Velocity (ft/sec)	Energy (Joules)	Absorbed Energy (Joules)	%
LG646	500 Zylon	A	6/24/2007	8	326.35	1.53	2.32	-5.780108	915.33	12701.03	842.34	10756.19	1944.842	0.153125
LG647	500 Zylon	A	6/27/2007	8	322.73	-4.26	24.48	-1.861686	929.78	12959.84	869.3695	11330.47	1629.366	0.125724

Table 4. Low Tension Test Results

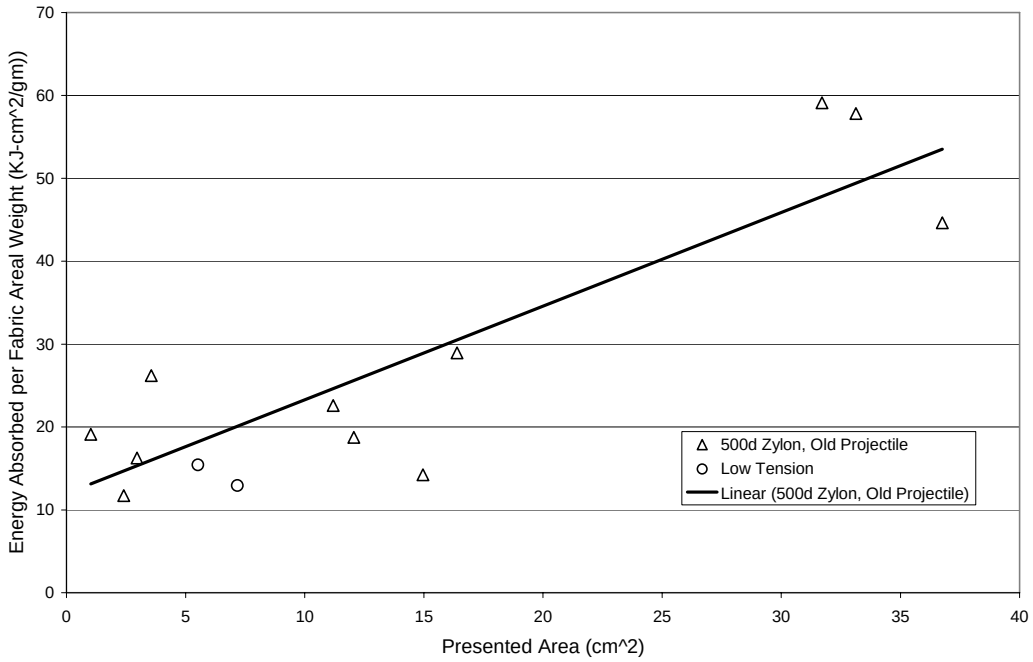

Figure 9. Comparison of Energy Absorbed by Low Tension Specimens and Nominal Tension Specimens

4. DISCUSSION AND CONCLUSIONS

The test configuration described here was designed to be somewhat representative of fabric containment systems used in jet engines, while maintaining repeatability and simplicity in the test. The results show that under the conditions of this test, Zylon is able to absorb over twice the energy than Kevlar when compared on an overall weight basis. The normalized energy absorbed is relatively insensitive to the number of layers of material. These results are consistent with results of Phase I of this study [2]. This allows for a fairly simple design procedure if the assumption is made that the amount of energy absorbed per unit weight is independent of the number of layers of material.

Except in cases where the yaw angle was high, the heavier weight Zylon material performed better than the lighter material, for the same overall weight. This is consistent with the results of Phase I. The energy absorbed by the fabric when normalized by the overall areal weight of the fabric ring is approximately linearly related to the presented area of the projectile at impact and, within the parameters of this study, is independent of the actual shape of the projectile.

The data presented here were taken using Zylon that had been stored for several months under normal laboratory conditions, without exposure to extreme temperature and humidity. It has been reported widely that the performance of Zylon degrades significantly under certain conditions of temperature and humidity which are likely to be

encountered in many applications. However these results indicate that degradation in the mechanical properties of Zylon occurs even under favorable conditions. The deterioration of strength over time seen in the current Zylon fabric makes the fabric impractical for long term use in engine containment systems.

The limited testing performed under conditions of no fabric tension indicate that there is no significant difference in energy absorption between the two tested conditions. However, this should be validated by additional testing.

The results for both Zylon and Kevlar presented here represent a useful set of data for the purposes of establishing both empirical and numerical models for predicting the response of fabrics under conditions simulating those of a jet engine blade release situations.

5. REFERENCES

1. Rajan, S.D., Mobashir, B., Sharda, J., Yanna, V., Deenadaylu, C., Lau, D and Shah, D, "Explicit Finite Element Modeling of Multi-layer Composite Fabric for Gas Turbine Engine Containment Systems. Part 1 – Static Tests and Modeling", Final Report, DOT/FAA/AR-04/40/P1, Nov., 2004.
2. Pereira, J.M., and Revilock, D.M., "Explicit Finite Element Modeling of Multi-layer Composite Fabric for Gas Turbine Engine Containment Systems. Part 2 – Ballistic Impact Testing", Final Report, DOT/FAA/AR-04/40/P2, Nov., 2004.
3. Simons, J., Erlich, D. and Shockey, D., "Explicit Finite Element Modeling of Multi-layer Composite Fabric for Gas Turbine Engine Containment Systems. Part 3: Model Development and Simulation of Experiments", Final Report, DOT/FAA/AR-04/40/P3, Nov., 2004.
4. Gomuc, R. "Explicit Finite Element Modeling of Multi-layer Composite Fabric for Gas Turbine Engine Containment Systems. Part 4: Model Simulation for Ballistic Tests, Engine Fan Blade-Out and Generic Engine", Final Report, DOT/FAA/AR-04/40/P4, Nov., 2004.
5. "LS-DYNA Theoretical Manual," Livermore Software Technology Corp., Livermore CA, 1998.
6. "ABAQUS/Explicit User's Manual," ABAQUS, Inc., Pawtucket RI, 2003.
7. Wong, A.K and Connors, M.L., "A Literature Survey on Correlation of Laboratory Tests and the Ballistic Resistance of Rolled Homogeneous Steel and Aluminum Armors," *Technical Report AMMRC SP 72-10*, Army Materials and Mechanics Research Center, Watertown MA, Sep 1971.
8. Clifton, R.J., "Response of Materials Under Dynamic Loading," *International Journal of Solids and Structures*, Vol, 37, pp. 105-113, 2000.
9. Johnson, G.R. and Cook, W.H., "Fracture Characteristics of Three Metals Subjected to Various Strains, Strain Rates, Temperatures and Pressures," *Engineering Fracture Mechanics*, Vol. 21(1), pp. 31-48, 1985.
10. Roylance, D. and Wang, S.S., "Penetration Mechanics of Textile Structures in Ballistic Materials and Penetration Mechanics," R.C. Laible, ed., Elsevier, 1980.

11. Cunniff, P.M., “A Semi-empirical Model for the Ballistic Impact Performance of Textile-based Personnel Armor,” *Textile Research Journal*, Vol. 56, pp. 45-60, 1996.
12. Figucia, F., “Energy Absorption of Kevlar Fabrics Under Ballistic Impact,” *Technical Report A090390*, Defense Technical Information Center, 1980.
13. Tabiei, A. and Ivanov, I., “Computational Micro-mechanical Model of Flexible Woven Fabric for Finite Element Impact Simulation,” *International Journal of Numer. Meth., Engng*, Vol. 53, pp. 1259-1276, 2002.
14. Lim, C.T. , Shim, V.P.W. and Ng, Y.H., “Finite-element Modeling of the Ballistic Impact of Fabric Armor,” *International Journal of Impact Engineering*, Vol. 28, pp. 13-31, 2003.
15. Zohdi, T.I., “Modeling and Simulation of Progressive Penetration of Multilayered Ballistic Fabric Shielding,” *Comput. Mech.* Vol. 29(1), pp. 61-67, 2002.
16. Scala, P.E., “A Brief History of Composites in the U.S.—The Dream and the Success,” *JOM*, Vol. 48(2), pp. 45-48, 1996.
17. Stotler, C.L., “Development of Advanced Lightweight Containment Systems,” *NASA CR-165212*, National Aeronautics and Space Administration, 1981.
18. Shockey, D.A., Erlich, D.C and Simons, J.W., “Lightweight Fragment Barriers for Commercial Aircraft,” *18th International Symposium on Ballistics*, San Antonio TX, 15-19 Nov, 1999.
19. Pereira, J.M., Roberts, G.D. and Revilock, D.M., “Elevated Temperature Ballistic Impact Testing of PBO and Kevlar Fabrics for Application in Supersonic Jet Engine Fan Containment Systems,” *NASA TM-107532*, Aug 1997.
20. Simons, J.W., Erlich, D.C. and Shockey, D.A., “Explicit Finite Element Modeling of Multi-layer Composite Fabric for Gas Turbine Engine Containment Systems,” FAA report in press.
21. Cunniff, P.M., “An Analysis of the System Effects in Woven Fabrics under Ballistic Impact”, *Textile Research Journal*, 62(9), 1992.

Appendix A. Procedure for Computing Euler Angles

Using the 3-D photogrammetry system the position of three points on the projectile and three points on a fixed background can be measured. The points on the fixed background are used to define unit orthogonal vectors ($\hat{I}_1, \hat{I}_2, \hat{I}_3$) in the laboratory system. The points on the projectile are used to define a moving system of unit orthogonal vectors attached to the projectile. At any time, the position of the projectile can be described as a translation plus a sequence of three rotations:

1. Roll (θ) about the projectile *x*-axis
2. Pitch (ψ) about the projectile rotated *y*-axis
3. Yaw (φ) about the projectile twice-rotated *z*-axis

For the purposes of defining the orientation of the projectile we can ignore the translation terms. Imagine the projectile initially in a position where the projectile coordinate system lines up with the lab coordinate system. The position of a point, *R*, on the projectile can be described by:

$$\vec{R} = r_1\hat{i}_1 + r_2\hat{i}_2 + r_3\hat{i}_3 = r_1\hat{I}_1 + r_2\hat{I}_2 + r_3\hat{I}_3 \qquad \text{(A1)}$$

Where ($\hat{i}_1, \hat{i}_2, \hat{i}_3$) are the unit vectors attached to the projectile. If the projectile is rotated by the angle θ about the laboratory *X* axis, the vector $\vec{R}$ becomes $\vec{R}'$, given by

$$\vec{R}' = r_1\hat{e}_1 + r_2\hat{e}_2 + r_3\hat{e} = r_1'\hat{i}_1 + r_2'\hat{i}_2 + r_3'\hat{i}_3 \qquad \text{(A2)}$$

The unit vectors ($\hat{e}_1, \hat{e}_2, \hat{e}_3$) are the rotated unit vectors in the projectile (*x, y, z*) directions. These unit vectors can be found in terms of the ($\hat{i}_1, \hat{i}_2, \hat{i}_3$) vectors from

$$\begin{aligned}
\hat{e}_1 &= (\hat{e}_1 \cdot \hat{i}_1)\hat{i}_1 + (\hat{e}_1 \cdot \hat{i}_2)\hat{i}_2 + (\hat{e}_1 \cdot \hat{i}_3)\hat{i}_3 \\
\hat{e}_2 &= (\hat{e}_2 \cdot \hat{i}_1)\hat{i}_1 + (\hat{e}_2 \cdot \hat{i}_2)\hat{i}_2 + (\hat{e}_2 \cdot \hat{i}_3)\hat{i}_3 \\
\hat{e}_3 &= (\hat{e}_3 \cdot \hat{i}_1)\hat{i}_1 + (\hat{e}_3 \cdot \hat{i}_2)\hat{i}_2 + (\hat{e}_3 \cdot \hat{i}_3)\hat{i}_3
\end{aligned} \qquad \text{(A3)}$$

Inserting (A3) into (A2) and equating the vector components leads to

$$\begin{Bmatrix} r_1' \\ r_2' \\ r_3' \end{Bmatrix} = \begin{bmatrix} \hat{e}_1 \cdot \hat{i}_1 & \hat{e}_2 \cdot \hat{i}_1 & \hat{e}_3 \cdot \hat{i}_1 \\ \hat{e}_1 \cdot \hat{i}_2 & \hat{e}_2 \cdot \hat{i}_2 & \hat{e}_3 \cdot \hat{i}_2 \\ \hat{e}_1 \cdot \hat{i}_3 & \hat{e}_2 \cdot \hat{i}_3 & \hat{e}_3 \cdot \hat{i}_3 \end{bmatrix} \cdot \begin{Bmatrix} r_1 \\ r_2 \\ r_3 \end{Bmatrix} \qquad \text{(A4)}$$

In terms of the rotation angle, θ, this is

$$\begin{Bmatrix} r_1' \\ r_2' \\ r_3' \end{Bmatrix} = \begin{bmatrix} 1 & 0 & 0 \\ 0 & \cos(\theta) & -\sin(\theta) \\ 0 & \sin(\theta) & \cos(\theta) \end{bmatrix} \cdot \begin{Bmatrix} r_1 \\ r_2 \\ r_3 \end{Bmatrix} \qquad \text{(A5)}$$

Assume that the projectile goes through another rotation, ψ, about the projectile *y*-axis, so that the vector $\vec{R}'$ becomes $\vec{R}''$ and the unit vectors $(\hat{e}_1, \hat{e}_2, \hat{e}_3)$ become $(\hat{f}_1, \hat{f}_2, \hat{f}_3)$. The vector $\vec{R}''$ can be written as:

$$\vec{R}'' = r_1\hat{f}_1 + r_2\hat{f}_2 + r_3\hat{f}_3 = r_1^*\hat{e}_1 + r_2^*\hat{e}_2 + r_3^*\hat{e}_3 = r_1''\hat{i}_1 + r_2''\hat{i}_2 + r_3''\hat{i}_3 \qquad \text{(A6)}$$

Similar to Eqn. (A3), the components of $\hat{f}$ can be written in terms of the components of $\hat{e}$ as:

$$\begin{aligned} \hat{f}_1 &= (\hat{f}_1 \cdot \hat{e}_1)\hat{e}_1 + (\hat{f}_1 \cdot \hat{e}_2)\hat{e}_2 + (\hat{f}_1 \cdot \hat{e}_3)\hat{e}_3 \\ \hat{f}_2 &= (\hat{f}_2 \cdot \hat{e}_1)\hat{e}_1 + (\hat{f}_2 \cdot \hat{e}_2)\hat{e}_2 + (\hat{f}_3 \cdot \hat{e}_3)\hat{e}_3 \\ \hat{f}_3 &= (\hat{f}_3 \cdot \hat{e}_1)\hat{e}_1 + (\hat{f}_3 \cdot \hat{e}_2)\hat{e}_2 + (\hat{f}_3 \cdot \hat{e}_3)\hat{e}_3 \end{aligned} \qquad \text{(A7)}$$

The twice rotated vector $\vec{R}''$ can then be written in terms of the unit vectors $(\hat{e}_1, \hat{e}_2, \hat{e}_3)$:

$$\begin{aligned} \vec{R}'' = &\left[r_1(\hat{f}_1 \cdot \hat{e}_1) + r_2(\hat{f}_2 \cdot \hat{e}_1) + r_3(\hat{f}_3 \cdot \hat{e}_1)\right] \cdot \hat{e}_1 + \left[r_1(\hat{f}_1 \cdot \hat{e}_2) + r_2(\hat{f}_2 \cdot \hat{e}_2) + r_3(\hat{f}_3 \cdot \hat{e}_3)\right] \cdot \hat{e}_2 + \\ &\left[r_1(\hat{f}_1 \cdot \hat{e}_3) + r_2(\hat{f}_2 \cdot \hat{e}_3) + r_3(\hat{f}_3 \cdot \hat{e}_3)\right] \cdot \hat{e}_3 \end{aligned} \qquad \text{(A8)}$$

Equating this to the components of $\hat{r}^*$ in Eqn. (A6) gives

$$\begin{Bmatrix} r_1^* \\ r_2^* \\ r_3^* \end{Bmatrix} = \begin{bmatrix} \hat{f}_1 \cdot \hat{e}_1 & \hat{f}_2 \cdot \hat{e}_1 & \hat{f}_3 \cdot \hat{e}_1 \\ \hat{f}_1 \cdot \hat{e}_1 & \hat{f}_2 \cdot \hat{e}_2 & \hat{f}_2 \cdot \hat{e}_2 \\ \hat{f}_1 \cdot \hat{e}_3 & \hat{f}_2 \cdot \hat{e}_3 & \hat{f}_3 \cdot \hat{e}_3 \end{bmatrix} \cdot \begin{Bmatrix} r_1 \\ r_2 \\ r_3 \end{Bmatrix} \qquad \text{(A9)}$$

In terms of the rotation angle ψ this is:

$$\begin{Bmatrix} r_1^* \\ r_2^* \\ r_3^* \end{Bmatrix} = \begin{bmatrix} \cos\psi & 0 & \sin\psi \\ 0 & 1 & 0 \\ -\sin\psi & 0 & \cos\psi \end{bmatrix} \cdot \begin{Bmatrix} r_1 \\ r_2 \\ r_3 \end{Bmatrix} \qquad \text{(A10)}$$

But the components of $\vec{R}''$ in the laboratory coordinate system can be given in terms of r_1^*, r_2^* and r_3^* using Eqn. (A6) and (A3):

$$\begin{Bmatrix} r_1'' \\ r_2'' \\ r_3'' \end{Bmatrix} = \begin{bmatrix} 1 & 0 & 0 \\ 0 & \cos(\theta) & -\sin(\theta) \\ 0 & \sin(\theta) & \cos(\theta) \end{bmatrix} \cdot \begin{Bmatrix} r_1^* \\ r_2^* \\ r_3^* \end{Bmatrix} \qquad \text{(A11)}$$

Substituting Eqn. (A11) into (A10) gives:

$$\begin{Bmatrix} r_1'' \\ r_2'' \\ r_3'' \end{Bmatrix} = \begin{bmatrix} 1 & 0 & 0 \\ 0 & \cos(\theta) & -\sin(\theta) \\ 0 & \sin(\theta) & \cos(\theta) \end{bmatrix} \cdot \begin{bmatrix} \cos\psi & 0 & \sin\psi \\ 0 & 1 & 0 \\ -\sin\psi & 0 & \cos\psi \end{bmatrix} \cdot \begin{Bmatrix} r_1 \\ r_2 \\ r_3 \end{Bmatrix} \qquad \text{(A12)}$$

Finally, let the projectile go through a third rotation, φ, about the twice rotated projectile *z*-axis, so that the vector $\vec{R}''$ is rotated to $\vec{R}'''$ given in the lab coordinate system by $\vec{R}''' = r_1''' \cdot \hat{i}_1 + r_2''' \cdot \hat{i}_2 + r_3''' \cdot \hat{i}_3$

Following a similar procedure that led to Eqn. (A12) leads to

$$\begin{Bmatrix} r_1''' \\ r_2''' \\ r_3''' \end{Bmatrix} = \begin{bmatrix} 1 & 0 & 0 \\ 0 & \cos\theta & -\sin\theta \\ 0 & \sin\theta & \cos\theta \end{bmatrix} \begin{bmatrix} \cos\psi & 0 & \sin\psi \\ 0 & 1 & 0 \\ -\sin\psi & 0 & \cos\psi \end{bmatrix} \begin{bmatrix} \cos\varphi & -\sin\varphi & 0 \\ \sin\varphi & \cos\varphi & 0 \\ 0 & 0 & 1 \end{bmatrix} \begin{Bmatrix} r_1 \\ r_2 \\ r_3 \end{Bmatrix} \qquad \text{(A13)}$$

or

$$\begin{Bmatrix} r_1''' \\ r_2''' \\ r_3''' \end{Bmatrix} = \begin{bmatrix} \cos\psi\cos\varphi & -\cos\psi\sin\varphi & \sin\psi \\ \cos\theta\sin\varphi + \sin\theta\sin\psi\cos\varphi & \cos\theta\cos\varphi - \sin\theta\sin\psi\sin\varphi & -\sin\theta\cos\psi \\ \sin\theta\sin\varphi - \cos\theta\sin\psi\cos\varphi & \sin\theta\cos\varphi + \cos\theta\sin\varphi\sin\psi & \cos\theta\cos\psi \end{bmatrix} \begin{Bmatrix} r_1 \\ r_2 \\ r_3 \end{Bmatrix}$$

(A14)

The unit vectors defining the projectile and laboratory coordinate systems were defined using markers placed in the high speed video field of view, as shown schematically in Figure A1. The unit vectors on the projectile were defined as

$$\hat{i}_1 = (\vec{r}_b - \vec{r}_a)/\left|(\vec{r}_b - \vec{r}_a)\right| \qquad \text{(A15)}$$

$$\vec{i}_2 = \frac{\left[(\vec{r}_c - \vec{r}_a)\times \hat{i}_1\right]}{\left|(\vec{r}_c - \vec{r}_a)\times \hat{i}_1\right|} \qquad \text{(A16)}$$

$$\hat{i}_3 = \hat{i}_1 \times \hat{i}_2 \qquad \text{(A17)}$$

The unit vectors in the laboratory coordinate system were defined as:

$$\hat{I}_1 = (\vec{r}_B - \vec{r}_A)/\left|(\vec{r}_B - \vec{r}_A)\right| \qquad \text{(A18)}$$

$$\hat{I}_3 = (\vec{r}_C - \vec{r}_A)/\left|(\vec{r}_C - \vec{r}_A)\right| \qquad \text{(A19)}$$

$$\hat{I}_2 = \hat{I}_3 \times \hat{I}_1 \qquad \text{(A20)}$$

Any vector, $\vec{R}$, in the laboratory coordinate system can be obtained from the components in the blade coordinate system:

$$\vec{R} = r_1\hat{i}_1 + r_2\hat{i}_2 + r_3\hat{i}_3 = R_1\hat{I}_1 + R_2\hat{I}_2 + R_3\hat{I}_3 \qquad \text{(A21)}$$

$$\begin{aligned}\vec{R} = {} & r_1\left[(\hat{i}_1\cdot\hat{I}_1)\cdot\hat{I}_1 + (\hat{i}_1\cdot\hat{I}_2)\cdot\hat{I}_2 + (\hat{i}_1\cdot\hat{I}_3)\cdot\hat{I}_3\right] + r_2\left[(\hat{i}_2\cdot\hat{I}_1)\cdot\hat{I}_1 + (\hat{i}_2\cdot\hat{I}_2)\cdot\hat{I}_2 + (\hat{i}_2\cdot\hat{I}_3)\cdot\hat{I}_3\right] \\ & + r_3\left[(\hat{i}_3\cdot\hat{I}_1)\cdot\hat{I}_1 + (\hat{i}_3\cdot\hat{I}_2)\cdot\hat{I}_2 + (\hat{i}_3\cdot\hat{I}_3)\cdot\hat{I}_3\right]\end{aligned} \qquad \text{(A22)}$$

and therefore

$$\begin{Bmatrix} R_1 \\ R_2 \\ R_3 \end{Bmatrix} = \begin{bmatrix} \hat{i}_1\cdot\hat{I}_1 & \hat{i}_2\cdot\hat{I}_1 & \hat{i}_3\cdot\hat{I}_1 \\ \hat{i}_1\cdot\hat{I}_2 & \hat{i}_2\cdot\hat{I}_2 & \hat{i}_3\cdot\hat{I}_2 \\ \hat{i}_1\cdot\hat{I}_3 & \hat{i}_2\cdot\hat{I}_3 & \hat{i}_3\cdot\hat{I}_3 \end{bmatrix} \cdot \begin{Bmatrix} r_1 \\ r_2 \\ r_3 \end{Bmatrix} \qquad \text{(A23)}$$

The matrix in Eqn. (23) can be easily computed and is the same as that in Eqn. (A14). Our procedure for computing the Euler angles was to compute the terms in the matrix of Eqn. (A23) from the positions of points *a, b, c, A, B, C*, utilizing Eqns. (A15) – (A20) and then equate the terms of that matrix with those of Eqn. (A14).

For example, equating component (1, 3) in the two matrices gives

$$\psi = \sin^{-1}(\hat{i}_3\cdot\hat{I}_1) \qquad \text{(A24)}$$

Using this result and equating components (1, 2) gives

$$\varphi = \sin^{-1}\left[-(\hat{i}_2 \cdot \hat{I}_1) \Big/ \cos(\psi) \right] \qquad \text{(A25)}$$

Using components (3, 3) and Eqn. (A24) gives

$$\theta = \cos^{-1}\left[(\hat{i}_3 \cdot \hat{I}_3) \Big/ \cos(\psi) \right] \qquad \text{(A26)}$$

Care must be taken since the above formulas do not have unique solutions on their own. For example $\sin(\theta) = \sin(180-\theta)$.

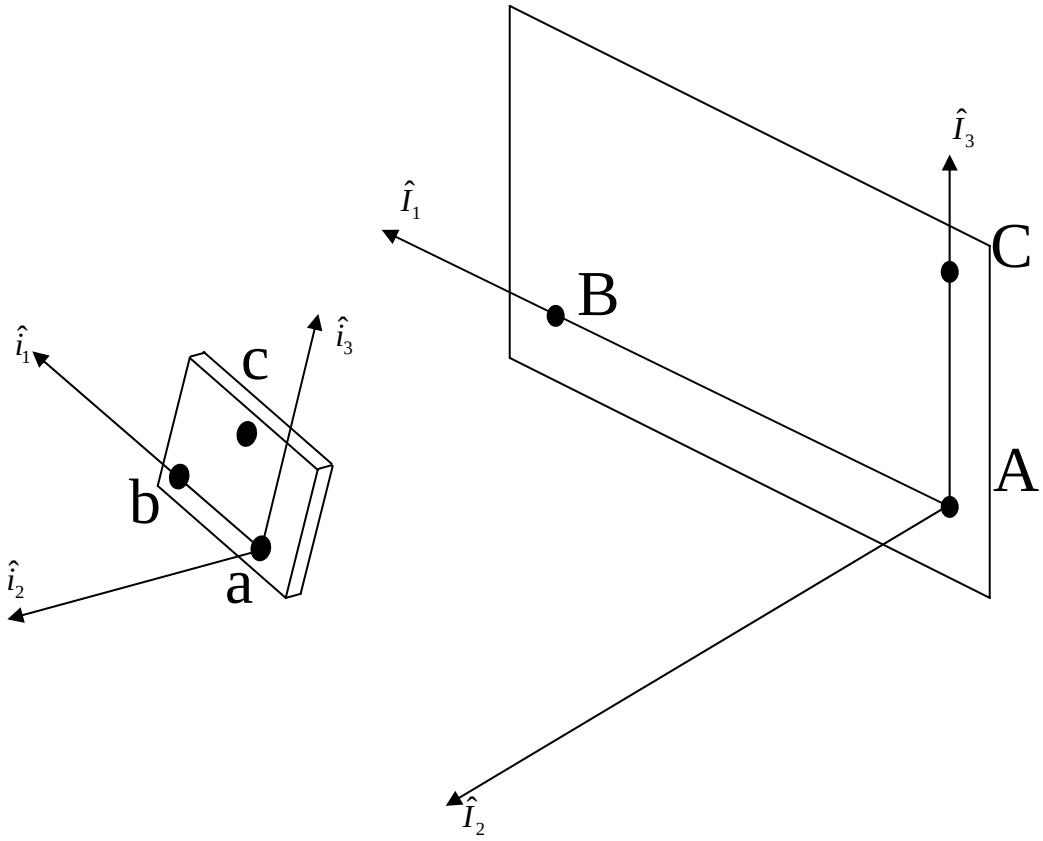

Figure A1. Projectile (left) and Background Coordinate Systems

Appendix B

Technical Report

Simple Tension Test Results:

Evaluating NASA's Zylon AS 1500D Fabric

Dept. of Civil Engineering

Arizona State University

Tempe, AZ 85287

February 2006

Overview

Tension tests of the NASA Zylon 1500D fabrics were carried out to find out the fabric properties. Questions were raised about the NASA ballistic test results involving Zylon 1500D fabric from Phase I of this research. The recent Phase II NASA ballistic test results showed a decrease in energy absorption from the Phase I tests. These tension tests were conducted at Arizona State University (ASU) to try to understand the differences in the NASA test results. The basic properties of the fabric as tested are shown in Table 1.

Table 1 Specimen Properties for Zylon AS–1500D

Yarn Count	Bulk Density (lb/in^3)	Linear Density (lb/in)	c/s Area per Yarn (in^2)	Specimen Size (in)
17 x 17	0.00567358	$9.13395(10^{-7})$	$1.61(10^{-4})$	2.5 x 10.25

Test Results

All samples referred to in this report were manufactured by Toyobo. Warp and fill yarns were all taken from fabric weaved at Lincoln Fabrics Ltd. The samples referred to as NASA samples were woven in March 2002 and used by NASA in the Phase I ballistic testing. In addition, the Boeing tested samples [1] mentioned in this report were all taken from the same lot of weaved fabric used in the NASA Phase 1 ballistic testing. The samples referred to as ASU samples were woven in June 2004 and used by NASA in the Phase II ballistic testing. All tests conducted at ASU reflect the warp direction properties of the fabric – warp direction is also referred to as the 1 direction. Figure 1 shows the stress-strain curves for four (NASA) replicates tested in Feb 2006. Figure 2 shows the stress-strain curves for five (ASU) replicates tested in Feb 2005. Tables 2, 3 and 4 contain the summary of the test results for the ASU Samples (Test Date Feb 2005), NASA Samples (Test Date Feb 2006), and the ASU Samples (Test Date Feb 2006) respectively.

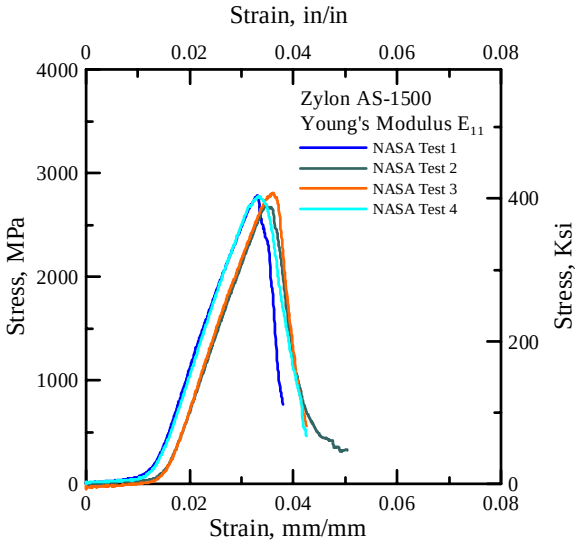

Figure 1. Stress-Strain Curves (E_{11}) for NASA Samples Tested in Feb 2006

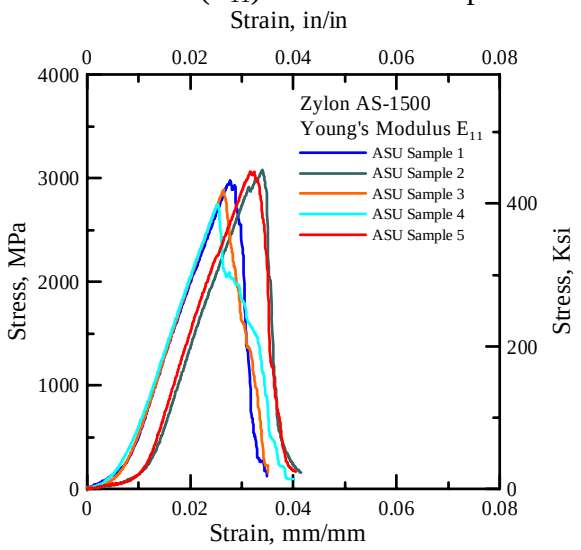

Figure 2. Stress-Strain Curves (E_{11}) for ASU Samples Tested in Feb 2005

The stiffness value is the highest slope in the pre-peak region of the stress-strain curve. The toughness value reflects the area under the stress-strain curve.

Table 2. Summary of Fabric Properties (ASU Zylon 1500D Samples)
Test Date: Feb 2005

	Sample ID	**Maximum Stress** (MPa)	**Toughness** (MPa)	**Stiffness, E** (MPa)
	1	3285	58.3	148083
	2	3412	62.7	152118

	3	3290	60.7	150966
	4	3088	69.7	145558
	5	3127	55.3	148475
Average		3240	61	149040
Std. Dev		132	5.4	2576

Table 3. Summary of Fabric Properties (NASA Zylon 1500D Samples)
Test Date: Feb 2006

	Sample ID	**Maximum Stress** (MPa)	**Toughness** (MPa)	**Stiffness, E** (MPa)
	1	2785	47.5	145404
	2	2699	49.4	141602
	3	2810	54.6	142927
	4	2776	53.6	149649
Average		2768	51	144896
Std. Dev		47.6	3.4	3539

Table 4. Summary of Fabric Properties (ASU Zylon 1500D Samples)
Test Date: Feb 2006

	Sample ID	**Maximum Stress** (MPa)	**Toughness** (MPa)	**Stiffness, E** (MPa)
	1	2978	44.2	144898
	2	3083	48.2	144482
	3	2888	44.2	148025
	4	2748	48.3	144507
	5	3064	52.4	149795
Average		2952	47.5	146341
Std. Dev		137.9	3.4	2432.5

Comparison of Tests Results

The test results show a noticeable decrease in the strength of the fabric with age. In a 12 month period, the maximum stress value shows a 9% decrease, the toughness a 22% decrease, and stiffness a small 2% decrease. Table 5 shows the properties obtained from various tests and sources for the Zylon 1500D fabric and the published fiber strength from Toyobo [1, 2]. It should noted that the Boeing values are from tests of a single warp or fill yarn whereas the ASU values reflect test results from a swatch of fabric.

Additional tests were run by Boeing on 500 denier Zylon samples from the same manufacturing lot. Table 6 summarizes the results which show the decrease in strength associated with the weaving process.

Table 5. Comparison of Fabric Properties Obtained From Various Sources

Data Source	Sample Description	Weave date	Test Date	Time (mo)	Max stress (MPa)	Toughness (MPa)	Stiffness (MPa)
ASU	1500D ASU (phase II) Warp	June 04	Feb 05	8	3240	61	149040
ASU	1500D ASU (phase II) Warp	June 04	Feb 06	20	2952	47.5	146341
Boeing	1500D NASA (phase I) Warp	Mar 02	Nov 02	8	3448		140556
Boeing	1500D NASA (phase I) Fill	Mar 02	Nov 02	8	3291		146035
ASU	1500D NASA (phase I) Warp	Mar 02	Feb 06	47	2768	51	144896
Toyobo	Web site fiber properties				5800		180000

Information in Table 5 is presented in a graphical form in figures 3 and 4. The effects of weaving and aging are shown in Table 6.

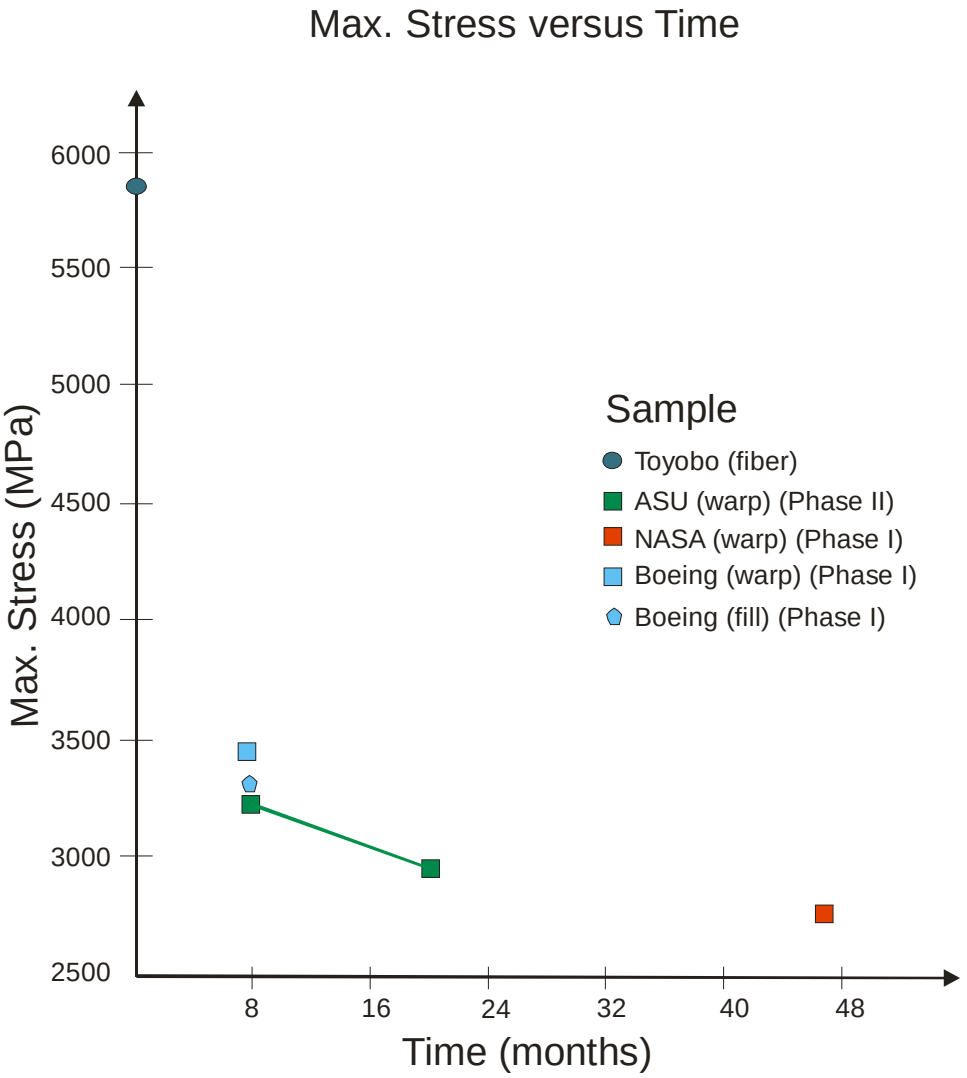

Figure 3. Variation in max. stress as a function of time

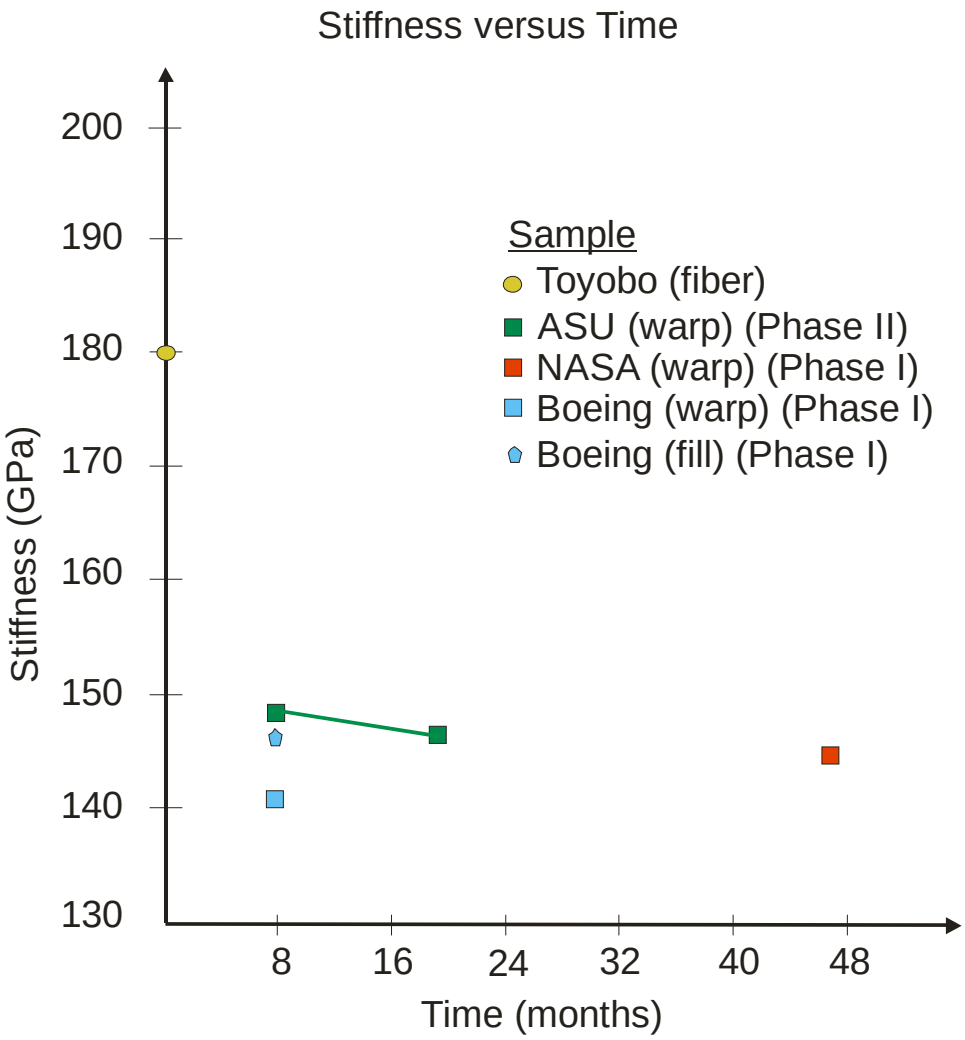

Figure 4. Variation in stiffness as a function of time

Table 6. Comparison of 500 Denier 35x35 Zylon Showing Effects of Weaving and Aging

Data Source	Sample Description	Weave date	Test Date	Time (mo)	Max stress (MPa)	Toughness (MPa)	Stiffness (MPa)
Boeing	500D (phase I) Warp	Mar 02	Nov 02	8	3135		142747
Boeing	500D (phase I) Fill	Mar 02	Nov 02	8	4232		155200
Boeing	500D (phase I) Virgin	Mar 02	Nov 02	8	4702		170295
Toyobo	Web site				5800		180000

	fiber properties						

Hypothesis Testing (t-Test)

Hypothesis testing (t-Test) is conducted on the ASU Test results to ascertain if the mean of the maximum stress value in the sample sets can be assumed to be the same or if they are different. The two hypotheses considered are as follows.

Null Hypothesis, H0: Mean of Samples 1 = Mean of Samples 2
Alternate Hypothesis, H1: Mean of Samples1 ≠ Mean of Samples 2

A 95% confidence level corresponding to a significance level as 0.05 is used in the following analysis. Two tests are carried out - the difference in mean between ASU Samples tested in Feb 05 and NASA Samples tested in Feb 06, and the difference in mean between ASU Samples tested in Feb 05 and ASU Samples tested in Feb 06.

Test 1 (ASU Samples tested in Feb 05 and NASA Samples tested in Feb 06)
Since, the standard deviation of maximum stress from NASA samples (47.6) is significantly less than the ASU samples' standard deviation (132), t-Test model for different standard deviations is adopted.

Sample size of ASU Samples tested in Feb 05, $n_1 = 5$
Sample size of NASA Samples tested in Feb 06, $n_2 = 4$

Standard deviation of ASU Sample set tested in Feb 05, $s_1 = 132.2$
Standard deviation of NASA Sample set tested in Feb 06, $s_2 = 47.6$

ASU Sample (max. stress), $m_1 = 3240.3\ MPa$
NASA Sample (max. stress), $m_2 = 2767.5\ MPa$

$$t_0 = \frac{(m_1 - m_2)}{\sqrt{\left(\frac{s_1^2}{n_1} + \frac{s_2^2}{n_2}\right)}}$$

(1)

$$\nu = \frac{\left(\frac{s_1^2}{n_1} + \frac{s_2^2}{n_2}\right)}{\left(\frac{\left(s_1^2/n_1\right)^2}{n_1 - 1} + \frac{\left(s_2^2/n_2\right)^2}{n_2 - 1}\right)}$$

(2)

$t_{\alpha/2,v}$ can found from the t-table where α is the significance level (taken as 0.05). Rejection criteria for NULL hypothesis is $|t_0| > t_{\alpha/2,v}$.

From above data, $t_0 = 7.417$ and $t_{\alpha/2,v} = 2.447$.

Since $|t_0| > t_{\alpha/2,v}$, the Null hypothesis H0 is rejected and alternate hypothesis H1 holds good. Thus the two samples have different mean values.

Test 2 (ASU Samples tested in Feb 05 and ASU Samples tested in Feb 06)
Since, the standard deviation of maximum stress for these two sample sets are identical, t-Test model for same standard deviation is adopted.

Sample size of ASU Samples tested in Feb 05, $n_1 = 5$.
Sample size of ASU Samples tested in Feb 06, $n_2 = 5$.

Standard deviation of ASU Samples tested in Feb 05, $s_1 = 132.2$.
Standard deviation of ASU Samples tested in Feb 06, $s_2 = 137.9$.

ASU Sample tested in Feb 05 (max. stress), $m_1 = 3240.3\ MPa$.
ASU Sample tested in Feb 06 (max. stress), $m_2 = 2952\ MPa$.

$$t_0 = \frac{(m_1 - m_2)}{s_p\sqrt{\left(\frac{1}{n_1} + \frac{1}{n_2}\right)}} \qquad \text{where} \quad s_p = \sqrt{\left(\frac{(n_1 - 1)s_1^2 + (n_2 - 1)s_2^2}{n_1 + n_2 - 2}\right)}$$

(3)

$$\nu = n_1 + n_2 - 2$$

(4)

$t_{\alpha/2,v}$ can found from the t-table where α is the significance level (taken as 0.05). Rejection criteria for Null hypothesis is $|t_0| > t_{\alpha/2,v}$

From above data, $t_0 = 3.37$ and $t_{\alpha/2,v} = 2.306$.

Since $|t_0| > t_{\alpha/2,v}$, NULL hypothesis H0 is rejected and alternate hypothesis H1 holds good. Thus the two samples have different mean values.

References

[1] Juris Verzemnieks, "Lightweight Ballistic Protection of Flight-Critical Components on Commercial Aircraft. Part 3: Zylon Yarn Tests", FAA report DOT/FAA/AR-05/45, P3, July 2005.

[2] http://www.toyobo.co.jp/e/seihin/kc/pbo/menu/fra_menu_en.htm